Deep Velocity Profiling using Lowered Acoustic Doppler Current Profiler: Bottom Track and Inverse Solutions

Martin Visbeck
Lamont-Doherty Earth Observatory of Columbia University, RT 9W, Palisades, NY 10964-8000
e-mail: visbeck@ldeo.columbia.edu

Short title: SUBMITTED TO J. ATMOS. OCEANIC TECHNOLOGY

Abstract. Lowered Acoustic Doppler Current Profilers (LADCPs) have matured from an experimental instrument to a quasi operational hydrographic tool to study ocean dynamics. The data processing, however, is still in a rather primitive state. Here, inverse solutions are presented that enhance the standard data processing by adding external constraints such as bottom referenced velocities profiles. The least squares framework also allows for simplified error analysis of the LADCP system.

1. Introduction

Direct velocity observations have allowed the study of many new aspects of ocean dynamics. For example the advent of vessel mounted acoustic Doppler current profiler (VMADCP) [e.g. *Joyce et al.*, 1982] has provided detailed insights into upper ocean dynamics. However, the limited range to a maximum depth of 300 to possibly 800 m (with reduced accuracy) left much to be desired. One way to overcome this limitation is to lower one or two self contained ADCP together with hydrographic sensor packages (which we will refer to as a CTD (Conductivity, Temperature and Depth recorder)), a method that has become known as LADCP profiling [see *Firing*, 1998, for a recent review].

The first LADCP cast was taken in 1989 at a site near Hawaii by *Firing and Gordon* [1990]. They showed that useful information was contained in the data, but argued that the expected errors of the system might be to large ($\sim 10\ cms^{-1}$) for many applications. A year later in 1990 *Fischer and Visbeck* [1993] used a similar system during a cruise in the tropical Atlantic. They had the advantage of simultaneous independent velocity profiles from a Pegasus system [*Spain et al.*, 1981] which allowed them to carefully evaluate the LADCP performance. They concluded that if care was taken LADCPs were able to reproduce much of the velocity field in comparison to the more accurate Pegasus system.

In recent years LADCPs were used extensively throughout the World Ocean Circulation Experiment (WOCE) era [*Firing*, 1998]and provided a wealth of useful top to bottom velocity profiles [e.g. *Beal and Bryden*, 1997; *Firing et al.*, 1998; *Fischer et al.*, 1996; *Hinrichsen and Lehmann*, 1994; *Schott et al.*, 1993; *Stramma et al.*, 1996; *Wijffels et al.*, 1998; *Wilson and Johns*, 1997]

The optimal choice of instrument hardware and parameter setting is still an open issue. Several factors have to be taken into account ranging from different acoustical properties of the ocean which themselves are a function of frequency, depth, and region;

instrument design, large or small beam angle and bandwidth. All those parameters contribute to the more fundamental tradeoff between range and accuracy. The goal is that a better fundamental understanding of the LADCP system will allow optimal hardware and parameter choices for the problem at hand.

More recently we have started to pay attention to the bottom reflected data of the LADCP system. King [pers comm, 1998] was the first to try the RDI built-in bottom track mode and reported good bottom tracked velocity profiles over a range of 50-250 m above the bottom even at water depths exceeding 3000 m. However, a fundamental questions arises: How can we optimally use this and other external information to improve the ocean velocity profile estimate?

In the following we briefly review the fundamentals of LADCP profiling (Section 2) and discuss aspects of LADCP sampling (Section 3). Different bottom track modes are reviewed and a new method derived that allows one to obtain "bottom track velocities" from the standard (non bottom track) LADCP data (Section 4). In Section 5 the basics of an alternative data processing scheme based on inverse methods is described. Its performance and advantages are discussed and summarized in Section 6.

2. Fundamentals of LADCP Profiling

The assumption behind the LADCP method is that one can use successive overlapping velocity profiles, which individually cover only a small fraction of the water column, to obtain a full ocean depth velocity profile (Fig. 1a). Each ADCP velocity observation can be interpreted as the sum of three parts:

$$U_{adcp} = U_{ocean} + U_{ctd} + U_{noise} \qquad . \tag{1}$$

U_{ctd} is the motion of the ADCP which is mounted on the CTD frame. A priori we know two aspects about U_{ctd}: The time integral over the whole cast (of duration T) is equal to the horizontal ship displacement during the cast (either due to drift or active

motion) DX_{ship}:

$$DX_{ship} = X^T_{ship} - X^0_{ship} = \frac{U_{ship}}{T} = \int_0^T U_{ctd}\ dt\ . \tag{2}$$

DX_{ship} can be inferred from the ships navigation system (e.g. high accuracy GPS or other navigation data). Secondly, U_{ctd} is assumed to vary slowly in relation to the time between pings (dt). In particular one assumes that it is constant for each individual ADCP profile (the time it takes for the acoustic pulse to travel through the water $\sim 0.2 - 0.5s$). **Figure 1.**

U_{ocean} represents the unknown velocity profile of the ocean. The ocean velocity profile is divided into nz elements each representative over a depth range dz, thus

$$H = nz\ dz \quad . \tag{3}$$

Typically U_{ocean} is assumed to be constant over the duration of the cast (T) and any variations will be interpreted as U_{noise}.

Finally, U_{adcp} represents the individual ADCP data which consist of nt velocity profiles. Each velocity profile consists of $nbin$ velocity estimates. Note, that the number of useful velocity data ($nbin$) is strongly a function of instrumental parameter and ocean acoustic conditions.

The goal is to partition the observed ADCP velocities into the two signals (U_{adcp} and U_{ocean}). This can be done 'sequentially' by considering some of the sampling aspects of the LADCP system. However, a more generic solution will be presented in Section 5.

2.1. Shear and Depth Averaged Velocities

U_{ocean} can be thought of as the sum of a depth average (barotropic) and depth varying (baroclinic) part:

$$U_{ocean}(z) = U_{ocean,barotropic} + U_{ocean,baroclinic}(z)\ . \tag{4}$$

As we will show, LADCP data without external information such as ships position or bottom track data can only constrain the baroclinic part of the ocean velocity.

The ADCP velocity profile (U_{adcp}) can also be thought of as the sum of two parts:

$$U_{adcp}(z) = U_{adcp,mean} + U_{adcp,variable}(z) \ . \tag{5}$$

Where $U_{adcp,mean}$ is a function of the CTD and ocean velocity. $U_{adcp,variable}$, however, and in particular its vertical derivative Us_{adcp}:

$$Us_{adcp}(z) = \frac{\partial U_{adcp,variable}}{dz} \tag{6}$$

only depends on the shear of the ocean velocity and is **independent** of the CTD motion. This aspect of the LADCP system can be exploited to obtain a baroclinic ocean velocity profile ($U_{ocean,baroclinic}$).

The classic method to process LADCP data works as follows [e.g. *Firing and Gordon*, 1990; *Fischer and Visbeck*, 1993]. First, the depth of the ADCP needs to be known. This can either be done by integrating the vertical velocity measured by the ADCP (Fig. 1)

$$z(t) = -\int_0^t w(t)dt \tag{7}$$

or by synchronization between the CTD pressure and ADCP data. Next, the vertical shear is computed for each individual ADCP profile. And all individual velocity shear estimates (Us_{adcp}) are averaged with respect to depth yielding an average top to bottom shear profile. *Fischer and Visbeck* [1993] discuss how careful shear data screening helps to improve the quality of the velocity profile. Finally, vertical integration of the shear profile results in a baroclinic ocean velocity profile ($U_{ocean,baroclinic}$).

Fischer and Visbeck [1993] also show how one recovers the barotropic ocean velocity ($U_{ocean,barotropic}$) by substituting the time integral of equation (4) into the time integral of equation (1):

$$\int_0^T U_{ocean,barotropic}dt = \int_0^T U_{adcp}dt - \int_0^T U_{ctd}dt - \int_0^T U_{ocean,baroclinic}dt - \int_0^T U_{noise}dt \ , \tag{8}$$

which can be simplified by assuming that U_{noise} has no systematic biases and its time

integral is small. Together with equation (2) we arrive at:

$$U_{barotropic} = \frac{1}{T}\left[\int_0^T U_{adcp}dt - \int_0^T U_{baroclinic}(z_{ctd}(t))dt\right] - U_{ship}\ . \tag{9}$$

Such an equation can be written for each of the *nbin* time series of U_{adcp} [*Fischer and Visbeck*, 1993].

Although U_{ctd} has not been used directly it can now be estimated from equation (1) including the unknown error U_{error}. In particular its time integral:

$$DX_{ctd}(t) = \int_0^t U_{ctd}(t')\ dt' \tag{10}$$

gives useful information about the relative position of the CTD package as a function of time (Fig. 1d).

Hitherto all LADCP software packages more or less follow this processing scheme. One of the fundamental shortcomings is that one bad velocity bin will cause two bad shear estimates. Moreover, if the ranges are short, say $nbin = 4$, only two shear estimates can be found by using a central difference method. Finally, it is not obvious how to make use of extra information, such as surface ship drift, ship board ADCP data or bottom referenced velocities to improve the estimated ocean velocity profile.

Before discussing an alternative data processing approach we will review some of the fundamental LADCP sampling issues.

3. LADCP Sampling

LADCP profiling is a compromise between range and resolution of individual ADCP velocity profiles versus their accuracy. The overall goal is clear: **long range and high accuracy at fine vertical resolution**. However, it is less clear how particular choices impact the final ocean velocity profile.

It seems helpful to define some fundamental non dimensional sampling ratios that can guide the LADCP user. It will become apparent that any hardware and parameter

choices depend on the users requirements of resolution and accuracy of the resulting ocean velocity profile.

Today's ADCP vendors offer a range of instruments with different base frequencies, beam angles and broad or narrow acoustic band width. Without going into much detail the tradeoffs are basically as follows: Maximum range is obtained by low frequencies, small beam angles and a narrow band width, while maximum accuracy requires exactly the opposite. There is no one obvious solution and several users favor range while others argue for accuracy. Even for a particular choice of hardware the user still can choose from a range of parameter settings. In the following we will discuss some of the consequences of these choices.

Most ADCPs can operate with different vertical resolutions, which is usually called the bin length (l_{bin}). The tradeoff here is accuracy versus resolution but also range. A long bin length has a higher accuracy and typically a larger range at the expense of vertical resolution. We will express the vertical resolution by a non dimensional number which compares the resolution of the ADCP (l_{bin}) to the desired resolution of the ocean velocity profile (dz):

$$R_{res} = \frac{dz}{l_{bin}} \quad . \tag{11}$$

For most applications R_{res} will be chosen to be order one which gives the highest possible accuracy for the desired final resolution.

One also needs to specify the time between pings (dt). Again there are tradeoffs: long ranges prohibit a high ping rate and high ping rates use more energy and internal memory. We will express the ping rate in terms of a vertical sampling length (dl) which is defined as the product of the sampling interval (dt) and a typical lowering speed ($\overline{w}$):

$$dl = \overline{w}\ dt \sim \frac{2H}{nt} \quad . \tag{12}$$

Here nt is the total number of ADCP profiles per cast and H is the depth of the desired velocity profile. The second non dimensional number compares this vertical sampling

length scale to the desired resolution of the ocean velocity profile (dz):

$$R_{samp} = \frac{dz}{dl} = \frac{dz}{dt\ \overline{w}} = \frac{dz\ nt}{2H} = \frac{nt}{2nz} \quad . \tag{13}$$

Typical values for R_{samp} are of order 10-50.

Finally, the ratio of the two compares the sampling length scale to the bin length:

$$R_{ens} = \frac{R_{res}}{R_{samp}} = \frac{dt\ \overline{w}}{l_{bin}} \quad . \tag{14}$$

R_{ens} can guide the users decision about how many individual profiles ($nens$) he might want to internally average into one ensemble. A conservative choice is to set R_{ens} to three resulting in:

$$nens = \frac{R_{ens}}{3} = \frac{dt\ \overline{w}}{3\ l_{bin}} \quad . \tag{15}$$

For a lowering speed of $\overline{w}$ =1 m s^{-1} , a bin length of l_{bin} = 10m and a ping interval of dt = 1 s we arrive at $nens \sim 3$. Thus from a sampling point of view no significant information is lost if 3 pings are averaged together to what is called one ensemble.

If energy is not a factor one would choose to set the time between pings as small as possible without compromising the range. A large number of individual pings will reduce the inherent observational noise and improve accuracy.

However, if the single ping accuracy is sufficient we would only need one velocity profile per vertical ADCP displacement of dz, the desired vertical resolution of the ocean velocity profile. Thus the maximum time between pings dt_{max} can be computed by setting R_{samp} to one:

$$dt_{max} = \frac{l_{bin}}{\overline{w}} \quad . \tag{16}$$

By the same argument one can begin the LADCP data processing with a data reduction stage: All profiles within the time it takes for the ADCP/CTD to cover a depth range dz are averaged together.

Note that we have omitted the discussion of straight forward first order quality control of the raw data to eliminate noise due to other acoustic sources, interference

between instruments, reflections from moving targets (fish) and bottom returns from previous pings and the like.

For a typical LADCP cast, where the down trace is followed by an up trace with possible stops to collect water samples, this yields $nta = 2\ dz$ super velocity profiles (nz profiles for each trace). The resulting reduced data set now has a sampling ratio (R_{samp}) of one.

The non dimensional sampling parameter (R_{ens}, R_{samp} and R_{res}) can help to describe the LADCP sampling with regards to the desired resolution of the final ocean velocity profile. We will revisit the sampling issue in the context of the problems dimension and final error discussion.

4. Bottom Referenced Absolute Velocities

The sea surface and ocean floor provide much larger back scatter compared to the oceans interior. Thus they can be detected from a large distance. As the LADCP approaches the bottom the strong reflections can be used to obtain a "bottom velocity" which is essentially the motion of the instrument ($-U_{ctd}$) relative to the stationary bottom. This method is called bottom tracking and often used for ship board ADCP applications. It allows to obtain absolute velocity profiles when the bottom is within the range of the instrument.

LADCP users have three options to obtain this valuable extra information. Firstly, there is the classical bottom track mode developed for ship board ADCP applications [*RDI-Primer*, 1989]. A powerful (bottom track) pulse is inserted between the regular (water) pings from which a bottom velocity and distance to the instrument is calculated. From the choices available this is the most accurate bottom velocity. However, it also requires significant extra power and in particular during deep casts only very few of those extra bottom track pulses will give useful bottom velocities when the bottom is within 20-300 m range of the ADCP.

Secondly, it is possible to diagnose the bottom velocity from the standard water pings. This post processing is possible if in addition to the velocity profiles the target strength (echo amplitude) was recorded. First the bin with maximum target strength needs to be located and its Doppler speed can then be interpreted as the desired bottom track velocity ($-U_{ctd}$).

More recently this procedure has been included into the real time LADCP processing for RDI workhorse ADCPs. This LADCP bottom track option consumes no extra power and has marginal computational overhead.

Figure (2) shows an example of bottom track velocities ($-U_{ctd}$) derived from the most accurate classical bottom track (open circles). The post processing analyses of the water ping data (solid dots) shows that both methods give similar results. Note, that the more powerful classical bottom track gives more good bottom track data due to its increased pulse length. However, the overall performance seems comparable. The mean difference between joint bottom track velocities was about 1.5 cm s^{-1} (Fig. 3). **Figure 2.**

Figure (3) shows the difference between the averaged bottom track velocities determined from the RDI-bottom track option (extra pulse) and the post processed method for 26 stations. There seems to be no significant mean difference and the scatter is within 2.5 cm s^{-1} (Fig. 3a). **Figure 3.**

Figure (4) shows the difference between the RDI-LADCP bottom track and the post processed bottom track using data from the north western Weddell Sea gyre. Note, that no extra pulse is required for either of the methods. However, the RDI-LADCP bottom track is available in real time. As expected both methods give similar results with a rms difference of about 1 cm s^{-1} . **Figure 4.**

In summary we have found little advantage in using the more accurate put power hungry extra bottom track pulse and recommend using the new built-in LADCP bottom track mode. If this is not an option one can always compute the bottom track velocities if both the velocity and target strength raw data are recorded.

We have shown that when a LADCP station extends to the bottom valuable extra information about the motion of the CTD package can be extracted. The profiles with good bottom referenced velocities can be used directly to obtain absolute velocity profiles near the bottom. Those profiles themselves have scientific payoff for the study of bottom currents and abyssal flows. They can also be compared to the lower part of the full ocean LADCP profile. However, what should one do if they disagree?

In the next section we describe an alternative LADCP processing scheme which is able to incorporate bottom referenced profiles and a range of other external information to improve the overall LADCP velocity profile.

5. A Linear Inverse Method to Process LADCP Data

The fundamental equation 1 can be thought of as set of linear equations of the form:

$$\mathbf{d} = \mathbf{G}\mathbf{m} + \mathbf{n} \tag{17}$$

where the vector $\mathbf{d}$ represents all ADCP velocities U_{adcp} from different depths within the water column. $\mathbf{n}$ represents the noise due to imperfect measurements ($\mathbf{d}$) and imperfect prediction of the true velocity field by $\mathbf{Gm}$. The unknown ocean velocity profile and the motion of the CTD package are combined into a single vector:

$$\mathbf{m} = \begin{bmatrix} \mathbf{m_{ctd}} \\ \\ \mathbf{m_{ocean}} \end{bmatrix} \tag{18}$$

which are related to the observations $\mathbf{d}$ by the model matrix $\mathbf{G}$.

The dimension of the problem (i.e. the dimension of the matrix $\mathbf{G}$) is defined by the number of velocity observations nd and the number of unknowns nm. The maximum number of observations is given by the number of velocity estimates per ping ($nbin$) times the number of profiles per cast (nt):

$$nd = nbin\ nt = 2\ nbin\ nz\ R_{samp} \tag{19}$$

If the profile extends to the bottom we typically lose (nd_{bottom}) velocity data:

$$nd_{bottom} = \frac{nbin^2 \; l_{bin}}{\overline{w} \; dt} = nbin^2 \; R_{res} \; R_{samp} \quad . \tag{20}$$

However, in most cases the number of bottom affected velocity is less than 10% of all data.

The unknowns are the sum of the ocean velocities plus the CTD velocities for each ensemble.

$$nm = nm_{ctd} + nm_{ocean} = nz + nt \tag{21}$$

The number of ocean velocities is $nz = H/dz$ velocity elements of thickness dz. The vertical resolution of the ocean velocity profile (dz) can be chosen by the user but should not be much smaller that the bin length (see section 3 $R_{res} \geq 1$). The number of unknown CTD velocities is ($nm_{ctd} = nt$) equal to the number of pings. One can immediately see that the system is formally over determined if the ratio of known to unknown (F) is greater than one (assuming that all data are independent):

$$F = \frac{nd}{nm} = \frac{nbin \; nt}{nz + nt} = \frac{nbin}{\left(\frac{1}{2 \; R_{samp}} + 1\right)} \quad . \tag{22}$$

Obviously F depends on the sampling strategy: Lets imagine that the ADCP has a very high ping rate and the lowering speed of the CTD is very slow ($R_{samp} \gg 1$). The resulting number of ADCP profiles nt will be much larger than the number of desired ocean velocity data nz and $F \sim nbin$. This shows that eventually the accuracy of the system is controlled by the number of (independent) vertical bins, i.e. the ADCP instrument range.

In the limit of a rather high lowering speed and slow ADCP ping rate that still allows for useful sampling ($R_{samp} \sim 1$) gives only one ADCP profile for each desired ocean velocity depth cell. Thus nt is two times nz (one U_{ctd} for each depth cell dz of the up and down cast). For this low sampling limit F approaches 2/3 $nbin$ which is not very different from the other limit. Thus LADCP systems with a range of more than two velocity bins ($nbin > 2$) are formally over determined.

5.1. A Simple Case

Lets consider a simple case to illustrate the set of linear equations 17. An ADCP is lowered with a constant vertical velocity to the bottom of the ocean and back to the surface (Fig. 1). The LADCP parameter are chosen such that $R_{samp} = R_{res} = 1$. The water depth is $H = 10dz$ and the range of the instrument is $nbin = 3$. The instrument is looking towards the bottom. The number of unknown ocean velocities is $nz = 10$ and the total number of pings is $nt = 2\ nz\ R_{samp} = 20$. The number of water velocities is $nd - nd_{bottom} = nbin(nt - nbin\ R_{res}\ R_{samp}) = 45$. Thus the system has $nt + nz = 30$ unknowns and 45 equations.

The array of linear equations (17) has the form:

$$\mathbf{d} = \begin{bmatrix} u_{1,1} \\ u_{1,2} \\ u_{1,3} \\ u_{2,1} \\ \vdots \\ u_{3,1} \\ \vdots \\ u_{20,3} \end{bmatrix}, \quad \mathbf{m} = \begin{bmatrix} u_{ctd,1} \\ u_{ctd,2} \\ u_{ctd,3} \\ \vdots \\ u_{ctd,20} \\ - - - \\ u_{ocean,1} \\ u_{ocean,2} \\ u_{ocean,3} \\ \vdots \\ u_{ocean,10} \end{bmatrix}, \quad \mathbf{G} = \left\{ \begin{array}{ccccc|ccccc} 1 & 0 & 0 & \cdots & 0 & 1 & 0 & 0 & \cdots & 0 \\ 1 & 0 & 0 & \cdots & 0 & 0 & 1 & 0 & \cdots & 0 \\ 1 & 0 & 0 & \cdots & 0 & 0 & 0 & 1 & \cdots & 0 \\ 0 & 1 & 0 & \cdots & 0 & 0 & 1 & 0 & \cdots & 0 \\ \vdots & \vdots & \vdots & \ddots & \vdots & \vdots & \vdots & \vdots & \ddots & \vdots \\ 0 & 0 & 1 & \cdots & 0 & 0 & 0 & 1 & \cdots & 0 \\ \vdots & \vdots & \vdots & \ddots & \vdots & \vdots & \vdots & \vdots & \ddots & \vdots \\ 0 & 0 & 0 & \cdots & 1 & 0 & 1 & 0 & \cdots & 1 \end{array} \right\}. \tag{23}$$

The full model matrix $\mathbf{G}$ is displayed in figure (5). Note that the model matrix is very sparse which can be exploited to solve the problem efficiently. In the following we will discuss the least squares solution of a set of linear equations. **Figure 5.**

5.2. Interior Solution

Equations of the form as show in (17) can be solved by least squares methods. One searches for solutions ($\mathbf{m}$) that minimizes the squared difference between the data ($\mathbf{d}$) and their prediction ($\mathbf{d_{pre}} = \mathbf{G m_{est}}$). Solutions for overdermind systems of linear equations are well known [for example *Menke*, 1989].

$$\mathbf{m_2}^{est} = \left[\mathbf{G^T G}\right]^{-1} \mathbf{G}^T \mathbf{d} \quad , or \tag{24}$$

$$\mathbf{m_1}^{est} = \mathbf{G}^T \left[\mathbf{G G^T}\right]^{-1} \mathbf{d} \tag{25}$$

Where $\mathbf{m_2^{est}}$ represents the familiar least square solution (L_2 norm) and $\mathbf{m_1^{est}}$ is a more robust estimator (L_1 norm) when noisy data are expected. The prediction error using the L_2 norm is given by: $E = \sum_{i=1}^{N} (d_i - d_i^{pre})^2$ and for the L_1 norm is: $E = \left[\sum_{i=1}^{N} |d_i - d_i^{pre}|\right]^2$.

Note, that $\mathbf{G G^T}$ given by the simple case (eq. 23 and Fig. 5) can not be inverted because the unknowns ($\mathbf{m}$) are not linear independent. This reflects the fact that LADCP data by themselves can only give the baroclinic ocean velocity profile without constraining the mean (see section 2). However, we can demand that the sum of all ocean velocities ($\sum \mathbf{m_{ocean}}$) be equal to zero:

$$\hat{\mathbf{d}} = \begin{bmatrix} \mathbf{d} \\ 0 \end{bmatrix}; \quad \hat{\mathbf{G}} = \left[\begin{array}{ccccc|ccccc} & & & & & & & & & \\ & & & \mathbf{G} & & & & & & \\ & & & & & & & & & \\ 0 & 0 & 0 & \cdots & 0 & w & w & w & \cdots & w \end{array}\right] \quad . \tag{26}$$

The magnitude of w controls how close the mean ocean velocity will be to zero.

Now the problem is well posed and one can obtain an inverse solution. In some cases it might be helpful to weight each equation by its expected error . We had good success by using the size of the correlation velocity as a predictor for the relative quality of each velocity measurement. Note, that we have purposefully chosen to multiply each observation ($\mathbf{d}(n)$) and associated row of the model matrix ($\mathbf{G}$) with their respective weight rather than applying a weight matrix during the solution. This allows us to use

faster algorithm to find the solution. For example we can solve

$$\mathbf{m_{chol}}^{est} = backwardsub(\mathbf{R}, forwardsub(\mathbf{R^T}, \mathbf{G^T d})) \tag{27}$$

using

$$\mathbf{R} = chol(\mathbf{G^T G}), \tag{28}$$

where *chol* denotes the Cholesky factorization:

$$A = chol(B)\ , with \quad A^T A = B\ . \tag{29}$$

The functions $fowardsub$ and *backwardsub* solve lower and upper triangular sets of linear equations.

5.3. Barotropic Constraint

One of the advantages of solving the LADCP problem using linear least squares methods is that additional information can easily be added to constrain the solution. For example if good ships navigation exists we can prescribe the time average of the unknown package motion (U_{cdt}, equation 2). This will add one row to the equation array:

$$\hat{\mathbf{d}} = \begin{bmatrix} \mathbf{d} \\ w\ U_{ship} \end{bmatrix}; \quad \hat{\mathbf{G}} = \left[\begin{array}{cccccc|ccccc} & & & & & & & & & & \\ & & & & & \mathbf{G} & & & & & \\ w\frac{dt_1}{T} & w\frac{dt_2}{T} & w\frac{dt_3}{T} & \cdots & w\frac{dt_{nprof}}{T} & & 0 & 0 & 0 & \cdots & 0 \end{array}\right] . \tag{30}$$

Where dt_n denotes the time between subsequent package velocities (U_{ctd}) and w is a weight that controls how strong the solution is expected to obey this constraint. Note, that this constraint should be used instead of equation (26).

5.4. Bottom Track

It is also possible to include the bottom referenced $U_{cdt,bottom}$ as a constraint. For each bottom track velocity one equation can be added of the form:

$$\hat{\mathbf{d}} = \begin{bmatrix} \mathbf{d} \\ wU_{ctd,bottom} \end{bmatrix}; \quad \hat{\mathbf{G}} = \left[\begin{array}{ccccc|ccccc} & & & \mathbf{G} & & & & & & \\ 0 & 0 & w & \cdots & 0 & 0 & 0 & 0 & \cdots & 0 \end{array}\right] \quad . \tag{31}$$

We can control the strength of the constraint by the weight w.

Alternatively one can add for each of the velocity estimates where a bottom referenced velocity exists a line of the form:

$$\hat{\mathbf{d}} = \begin{bmatrix} \mathbf{d} \\ w(U_{adcp} - U_{ctd,bottom}) \end{bmatrix}; \quad \hat{\mathbf{G}} = \left[\begin{array}{ccccc|ccccc} & & & \mathbf{G} & & & & & & \\ 0 & 0 & 0 & \cdots & 0 & 0 & 0 & w & \cdots & 0 \end{array}\right] \quad . \tag{32}$$

Both forms are valid with slight differences in the error propagation.

5.5. Smoothness

In a similar matter we can demand that the estimated ocean velocity profile is smooth by adding a standard smoothness constraint:

$$\hat{\mathbf{d}} = \begin{bmatrix} \mathbf{d} \\ 0 \\ 0 \\ \vdots \\ 0 \end{bmatrix}; \quad \hat{\mathbf{G}} = \left[\begin{array}{ccccc|ccccc} & & & & & \mathbf{G} & & & & \\ 0 & \cdots & 0 & -1w & 2w & -1w & 0 & \cdots & 0 \\ 0 & \cdots & 0 & 0 & -1w & 2w & -1w & \cdots & 0 \\ \vdots & \ddots & \vdots & \vdots & \vdots & \vdots & \vdots & \ddots & \vdots \\ 0 & \cdots & 0 & 0 & 0 & 0 & 0 & \cdots & -1w \end{array}\right] \quad . \tag{33}$$

The amount of smoothing of the ocean velocity profiles can be controlled by w.

By now it should be obvious how to add other constraints such as ship board ADCP velocities, or any other external information.

5.6. Properties of the LADCP system

So far we have outlined how the LADCP problem can be written as a set of linear equations. We have shown how other constrains can be added to improve the estimated

ocean velocity profile. The least squares framework also allows us to inspect how well the data constrain the solution: It is well known that the generalized inverse of the model matrix

$$\mathbf{G_2}^{-g} = \left[\mathbf{G^T G}\right]^{-1} \mathbf{G}^T \text{ , } or \tag{34}$$

$$\mathbf{G_1}^{-g} = \mathbf{G}^T \left[\mathbf{G G^T}\right]^{-1} \tag{35}$$

gives insights into the behavior of the solution. For example figure (6) maps one row of the generalized inverse into the depth time space of LADCP sampling as a function of range of the ADCP. This illustrates how the observed ADCP velocities contribute to one of the ocean velocities at an intermediate depth (bin 13) for a problem that is similar to the sample case (section 5.1) but with $nz = 20$. The right panels show the sum of the absolute weights as a function of depth. It is obvious that the solution is more locally constrained for larger ranges (*nbin*). Also note, that the velocity bins close to the instrument and the ones far away contribute most to the solution. This is by no means optimal. We expect that the quality of the velocity estimates deteriorates with distance from the transducer. Appropriate weighting (see section 5.1) with reduced confidence in the bins further away from the ADCP will spreads the influence more towards the middle bins. **Figure 6.**

We can also inspect the *importance* $\mathbf{n} = diag(\mathbf{N})$ of the data by inspecting the diagonal of the data resolution matrix:

$$\mathbf{N} = \mathbf{G G^{-g}} \text{ .} \tag{36}$$

Figure 7 plots the importance of the ADCP raw data for the sample case with $nz = 20$ for three different bin length. A short instrument range shows that the model will do a good job and fit every single data point well. Longer ranges will fit the individual data less well. However, the solution is then more robust against instrumental noise contained in the data. For many problems the importance of the data approaches the

ratio of known to unknowns F^{-1}. Recall that our simple case had $R_{samp} = 1$ and hence $F = 3/2\ nbin$ (using eqation 22). This typical value for $\mathbf{n_{typical}} = F^{-1} = \frac{2}{3nbin}$ is indicated by the dashed line. The best possible case with data covering the whole range of the ocean profile all the time ($nbin = nz$) will give an *importance* of $\mathbf{n_{opt}} = \frac{3}{2nz}$ as indicated by the dash-dotted line in figure 7. **Figure 7.**

A first guess for the error of the resulting velocity estimates can be obtained from the model parameter covariance matrix:

$$[cov\ (\mathbf{m_2})] = \sigma_d^2 \left[\mathbf{G^T G}\right]^{-1}\ , or \tag{37}$$

$$[cov\ (\mathbf{m_1})] = \sigma_d^2 \left[\mathbf{G G^T}\right]^{-1}\ , \tag{38}$$

under the (not very realistic) assumption that all data are independent and of equal uncertainty given by σ_d^2. Figure (8) shows the diagonal of $[cov\ (\mathbf{m})]$ for three different ranges (3,5, and 7 bins) for a profile of a total depth of 20 bins. The smallest error for the ocean velocities is expected close to half way between the bottom and the surface with increasing error towards the top and bottom. **Figure 8.**

Note that increased range reduces the mean error but more importantly the uncertainly at the top and bottom of the profile. Thus increased range will help to constrain the low vertical modes of the ocean velocity profile.

Next we can explore the impact of bottom referenced U_{ctd} data. Figure 9 shows the expected ocean and CTD velocity error for three scenarios. The top panel represents the estimated error for a solution which specifies the time mean U_{ctd} similar to figure 8. The next panel shows the expected velocity error when only bottom track data are used to constrain the solution. Notice the low error near the bottom and the almost linear increase towards the surface. Finally, the bottom panels shows how the bottom track improves upon the standard case. The error is reduced at all depths with the most significant improvement near the bottom. **Figure 9.**

Finally, let us inspect how an error in the raw velocity data U_{adcp} effects the final

velocity profile. The generalized inverse ($\mathbf{G}^{-\mathbf{g}}$) maps the raw data onto the velocities. Figure 10 shows how a spike in the data influences the final velocities $m'_{est} = \mathbf{G}^{-\mathbf{g}}\mathbf{d}'$. Two different cases of $\mathbf{d}'$ are chosen. The left column shows how a spike in the middle of one ADCP profile ($n_{spike} = nbin/2$) affects the solution for different values of the instrument range. The left column contrasts that with a spike at the end of one ADCP profile ($n_{spike} = nbin$). One can clearly see that noisy data at the beginning and/or end of individual ADCP profiles can introduce jumps in the resulting ocean velocity profile. In particular systems with short ranges are very sensitive to such noise. **Figure 10**

We conclude that expressing the LADCP system in terms of an array of linear equations allows us to gain valuable insight into the propagation of errors through the system.

6. Summary and Discussion

Two aspects of LADCP velocity profiling have been discussed: information obtained from bottom track data and an alternative data processing method using a linear least squares method. A subset of commercially available ADCPs can be lowered down to a depth of 6000m and allows us to obtain top to bottom velocity profiles in most parts of the worlds oceans. When ADCPs approach the bottom they are also capable to determine a bottom referenced velocity witch is directly measuring the motion of the instrument. This extra information can be used to interpret the lower part of an LADCP profile as absolute velocities. We have shown that instead of the power hungry extra bottom track pulse the bottom referenced velocity can be obtained from the standard water bins. A comparison between the two methods gave encouraging agreement.

However, what was less obvious is how to use this extra information to improve the overall quality of the final ocean velocity profiles. The main thrust of the paper is to outline the details of an alternative data processing scheme which recasts the LADCP problem as a set of linear equations that can be solved using standard least squares

methods. One of the great advantages of this approach is that it is very strait forward to include additional constraints such as bottom referenced velocities, smoothness of the solution and other aspects of the LADCP system. Moreover, solutions to linear equations are well understood and fundamental aspects of the LADCP system can be deduced. We have shown that increased range is a fundamental goal in order to reduce the overall error of the system. However, it also becomes clear, that noise in the first or last bins of each individual profile have a strong influence on the final solution.

In the following we will summarize the important findings of this paper by reviewing step by step the processing of one LADCP station.

6.1. LADCP data processing

We will use a station taken at $59^o30'$ S and $44^o21'$W just north of the Weddell Sea in the Southern Ocean obtained on board *Palmer* as part of the DOVETAIL project in August 1997. The ADCP hardware used were two RDI work horse LADCP systems which are pressure rated for ocean depths up to 6000m. The bin length of the 300 kHz units was set to $l_{bin} = 16$ m and the time between pings was 0.9 seconds. In order to save internal memory we averaged 3 successive profiles together to one ensemble. At this station the water depth was about 2000m and approximately $nt = 2400$ velocity profiles (ensemble) were taken within two hours. The two ADCPs were mounted on the CTD frame one looking upward and the other one looking downward to maximize the total range of velocity observations. Throughout most of the cast each instrument had a range of 160 m or approximately $nbin = 9$. Thus the total number of individual raw ADCP velocities is $2400 \cdot 9 = 21600$ for each instrument. The instruments were connected to each other and one was designated the mater and the other the slave. The slave listens to the master for the ping command and both units ping synchronously. Thus the dimension of the problem is about 40000 known raw data, 2400 unknown CTD velocities and 100 unknown ocean velocities with 20 m vertical resolution. A

brut force inversion of the problem would require to invert a 40000 by 2500 complex element matrix which alone will take up more than 100 MB of memory and several tens of minutes of CPU time on a 500MHz Pentium III processor. Note, that extrapolating this to a 6000m deep profile with single pings each 0.5 seconds could easily yield 100000 unknowns which would be impractical to invert on current generations of notebook computer. Thus a more clever treatment of the problem is advisable.

The vertical resolution (R_{res}, equation 11) of our problem is of order one as it should be. However, the sampling resolution (R_{samp}, equation 13) is 12. This suggests that after some first order raw data screening the number of ensembles can be significantly reduced. We have chosen to average all ADCP velocity data together as long as the CTD is within a 20m vertical bin. This reduces the number of ensembles from 2400 to 190 and now R_{samp} is about one.

The LADCP bottom track mode detected 370 bottom reflections within a range between 40 and 220 m off the bottom. The bottom track data were averaged in the same way as the water velocity data resulting in 21 average bottom track data. All profiles which have bottom track information were used to obtain a bottom referenced velocity profile by solving a set of inverse equations similar to equation (17 and 23) where the data are $U_{adcp} - U_{adcp,bottom}$. The model matrix $\mathbf{G_{bottom}}$ directly maps $U_{ocean,bottom}$ to the data since the CTD/ADCP velocity is known.

After adding the barotropic constrain, the bottom track and smoothing of the ocean velocity profile we end up with a dimension of 1560 equations to estimate 290 model parameter. The inverse solution plus some of the formal errors was found within 3 seconds of CPU time. The whole station was processed in less than one minute including reading of the raw data, finding the depth of each ping, raw data screening, reducing the data, preparing for the inverse solution, solving it and plotting and saving the results to disk. An illustration of the final ocean velocity for the particular station is given in figure 11. **Figure 11**

We conclude that solving the LADCP system as a set of linear equations is feasible with todays powerful personal computer systems.

Acknowledgments.

This work has benefited from numerous interactions amongst the LADCP user group (http://www.ldeo.columbia.edu/∼visbeck/ladcp) in particular Juergen Fischer, Christian Mertens, Gerd Krahmann, Bruce Huber, Lee Gordon, Brian King and Dan Torres. Brian King has kindly provided some bottom track LADCP profiles. The first version of the manuscript was prepared during a three month long visit at CSIRO, Hobart (winter 1998/99). I am indebt to Trevor McDougall for his hospitality and stimulating discussions as well as to Peter MacIntosh for providing me with a fast MATLAB based solver for linear equations. This is Lamont publication number ????.

References

Beal, L., and H. Bryden, Observations of an Agulhas undercurrent, *Deep Sea Res.*, *44*, 1715–1724, 1997.

Firing, E., Lowered ADCP developments and use in WOCE, *WOCE Newsletter*, *30*, 10–13, 1998.

Firing, E., and R. Gordon, Deep ocean acoustic Doppler current profiling., in *Proceedings of the IEEE Fourth Working Conference on Current Measurements, April 3-5, Clinton, Maryland*, pp. 192–201, 1990.

Firing, E., S. E. Wijffels, and P. Hacker, Equatorial subthermocline currents across the Pacific., *J. Geophys. Res*, *103*, 21,413–21,423, 1998.

Fischer, J., and M. Visbeck, Deep velocity profiling with self-contained ADCPs., *J. Atmos. Oceanic Technol.*, *10*, 764–773, 1993.

Fischer, J., F. Schott, and L. Stramma, Currents and transports of the Great Whirl-Socotra Gyre system during the summer monsoon, August 1993., *J. Geophys. Res*, *54*, 3573–3587, 1996.

Hinrichsen, H., and A. Lehmann, A comparison of geostrophic velocities and profiling adcp measurments in the iberian basin., *J. Atmos. Oceanic Technol.*, *11*, 901–914, 1994.

Joyce, T., T. Bitterman, and K. Prada, Shipboard acoustic profiling of upper ocean currents., *Deep-Sea Res.*, *29*, 903–913, 1982.

Menke, W., *Geophysical Data Analysis: Discrete Inverse Theory*, Academic Press, Inc. International Geophysics Series, 1989.

RDI-Primer, Acoustic Doppler Current Profilers Principles of operation: a practical primer., RD Instruments, San Diego, 1989.

Schott, F., J. Fischer, J. Reppin, and U. Send, On mean and seasonal currents and transports at the western boundary of the equatorial Atlantic., *J. Geophys. Res.*, *98*, 14,353–14,368, 1993.

Spain, P. F., D. L. Dorson, and H. T. Rossby, Pegasus: A simple, acoustically tracked velocity profiler, *Deep-Sea Res.*, *28A*, 1553–1567, 1981.

Stramma, L., J. Fischer, and F. Schott, The flow field off southwest India at 8N during the southwest monsoon of august 1993, *J. Mar. Res.*, *54*, 55–72, 1996.

Wijffels, S. E., M. M. Hall, T. Joyce, D. J. Torres, P. Hacker, and E. Firing, Multiple deep gyres of the western North Pacific: A WOCE section along 149E, *J. Geophys. Res.*, *103*, 12,985–13,009, 1998.

Wilson, W. D., and W. E. Johns, Velocity structure and transport in the Windward Island Passages, *Deep-Sea Res.*, *44*, 487–520, 1997.

Received _____

Draft 1.0 July 6, 2000

Figure Captions

Figure 1. LADCP velocity profiling: Top left panel shows an idealized LADCP cast in the depth - time dimension. The solid line represents the CTD depth as a function of time descending from the surface to the bottom and back to the surface. The shorter thick lines are examples of individual ADCP profiles with an unknown CTD velocity removed. The bottom left panel shows the raw vertical velocity of the package as a function of time. Note, that its time integral represents the depth of the package as shown in the top left panel. The upper right panel shows the estimated final ocean velocity profile of which small segments were observed by each individual ADCP profile. The bottom right figure shows the relative position of the package in the X-Y frame. The position of the start and when the CTD was at its deepest point are marked.

Figure 2. An example of the RDI bottom track (Broad Band 150kHz instrument) using an extra long bottom track pulse compared to the post processed bottom track using just the water bin data. (Data courtesy B. King, IOS Southampton, UK). a) scatter plot for both the u and v component and their mean differences for data pairs. Time series of individual bottom referenced velocities for the zonal b) and c) meridional component. Open circles represent the RDI bottom track solutions.

Figure 3. Difference between the built-in RDI and the post processed bottom track using just the water bin data. Each symbol represents the mean difference between the two bottom track velocities for one LADCP cats. The instrument used was a broad band RDI 150kHz system (B. King, IOS Southampton, UK provided the raw data)

Figure 4. Difference between the RDI LADCP and the post processed bottom track using just the water bin data. Each symbol represents the mean difference between the two bottom track velocities for one LADCP cats.

Figure 5. Model matrix **G** for the simple test case. The left part maps the observations to the unknown CTD motion and the right part is due to the ocean velocity. The top panel shows how many data points constrain each of the unknown. On average there are *nbin* estimates for the CTD motion and 2 *nbin* estimates for each ocean velocity.

Figure 6. Map of one row of the generalized inverse in the depth time plane. Panel a) uses the sample case with a range of 3 bins, b) 5 and c) 7 bins. Contributions are colored with the darkest value corresponding to the maximum, negative contributions have an additional dot. The smaller panels on the right show the sum of the absolute weights as a function of depth. Note that the sums are normalized by their maximum value.

Figure 7. Importance of the data ($\mathbf{n} = diag(\mathbf{G}\mathbf{G}^{-\mathbf{g}})$) is plotted versus the data vector. Note that the data vector has been sorted with regards to depth of the ADCP velocity data point. The respective panels indicate the dependence of **n** as a function of instrument range $nbin$ = 3, 5 and 7. The expected typical value for **n** is given by the dashed line and the best possible scenario by the dash dotted line (see text for details).

Figure 8. Expected error of the model parameter [$cov\mathbf{m}$] as a function of range. The vertical dashed line separates the estimated covariance for U_{ctd} from U_{ocean}.

Figure 9. Expected error of the model parameter for a LADCP simulation with $nz = 20$ and $nbin = 4$. Top panel show a solution which is constrained by specifying the time mean U_{ctd}. The middle panel only uses bottom track data in addition to the standard water velocities. The bottom panel uses both the bottom track and time mean U_{ctd} constrain.

Figure 10. Impact of a single spike in the ADCP velocity data on the solution as a function of range. The left column represents the influence of a spike in the middle of one ADCP profile while the right column shows how a spike at the end influences the model parameter estimates. All cases are for $nz = 20$ with variable range $nbin$=3,5, and 7.

Figure 11. Screen shot of the LADCP data processing software output.

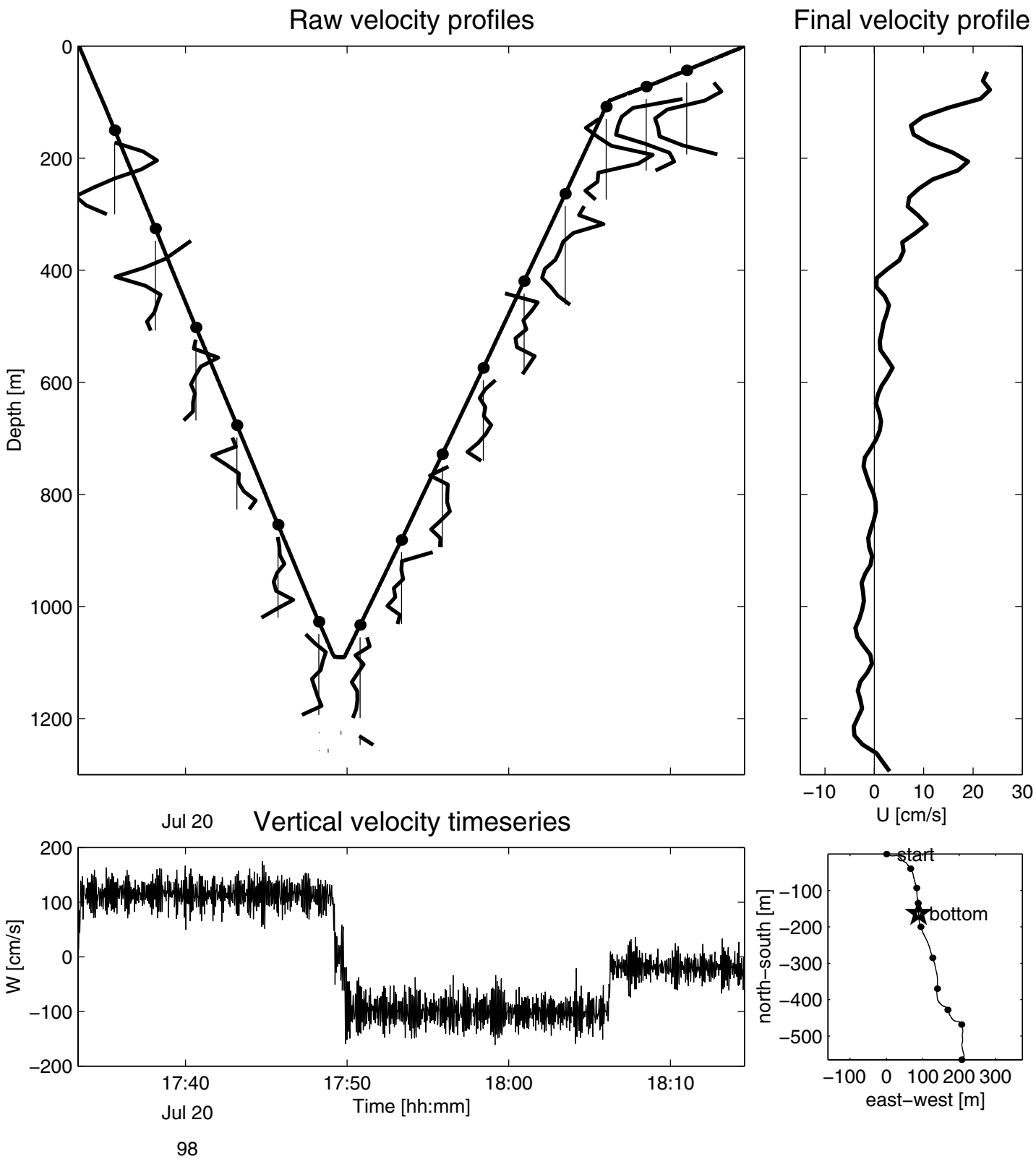
Raw velocity profiles
Final velocity profile
Depth [m]
0
200
400
600
800
1000
1200
−10
0
10
20
30
U [cm/s]
Jul 20
Vertical velocity timeseries
W [cm/s]
200
100
0
−100
−200
17:40
17:50
18:00
18:10
Jul 20
Time [hh:mm]
start
bottom
north−south [m]
−100
−200
−300
−400
−500
−100
0
100
200
300
east−west [m]
98

Figure 1

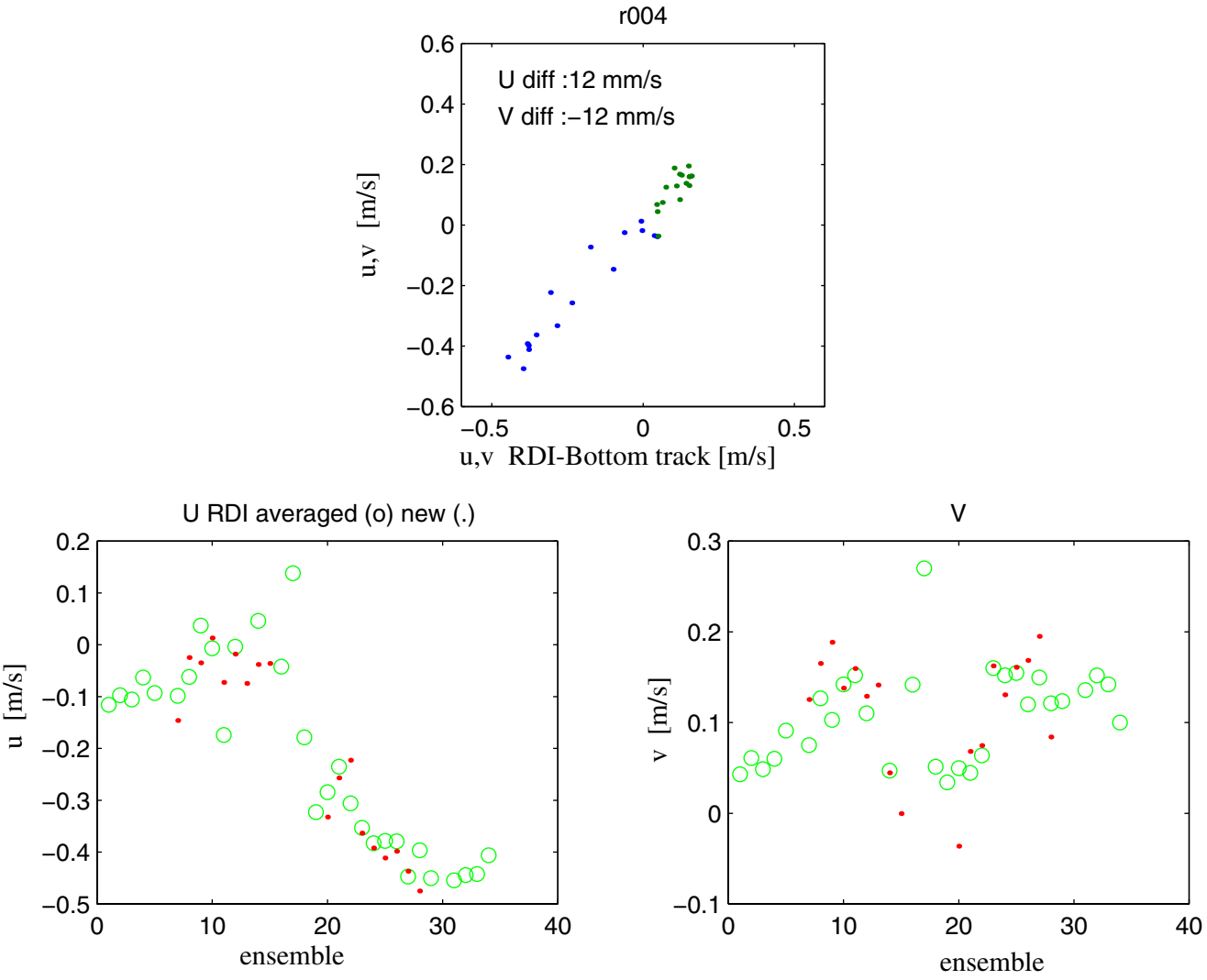
r004
U diff :12 mm/s
V diff :−12 mm/s
u,v [m/s]
u,v RDI-Bottom track [m/s]
U RDI averaged (o) new (.)
u [m/s]
ensemble
V
v [m/s]
ensemble

Figure 2

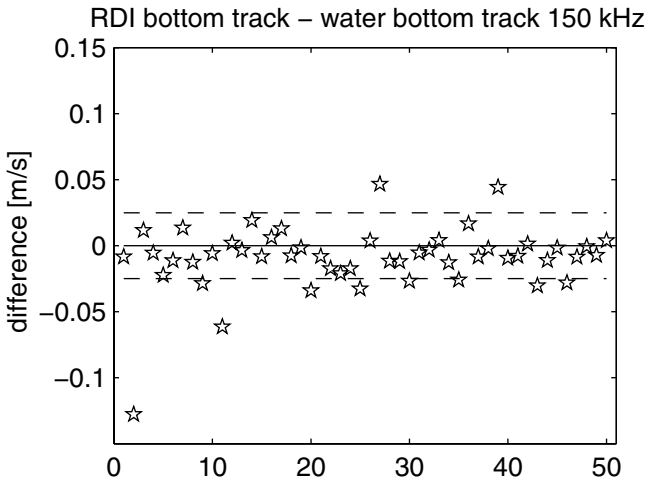
RDI bottom track – water bottom track 150 kHz
difference [m/s]
0.15
0.1
0.05
0
−0.05
−0.1
0
10
20
30
40
50

Figure 3

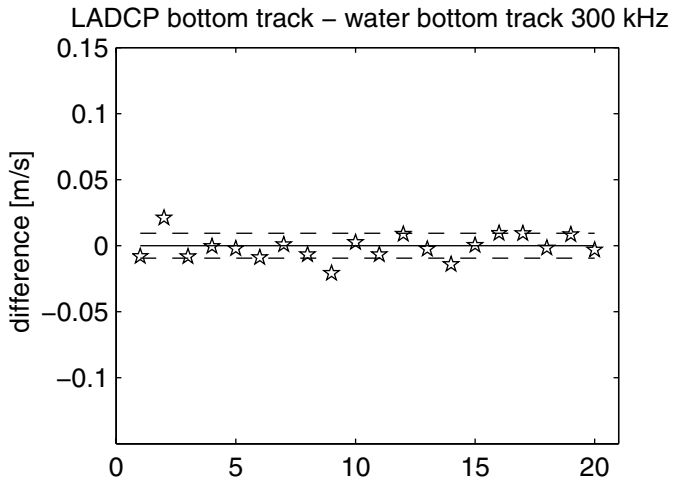
LADCP bottom track – water bottom track 300 kHz
difference [m/s]
0.15
0.1
0.05
0
−0.05
−0.1
0
5
10
15
20

Figure 4

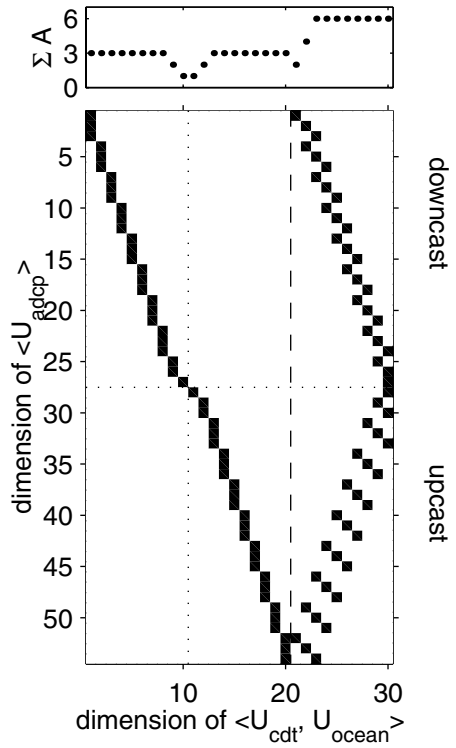
Σ A
6
3
0
5
10
15
20
25
30
35
40
45
50
dimension of <U adcp >
downcast
upcast
10
20
30
dimension of <U cdt, U ocean>

Figure 5

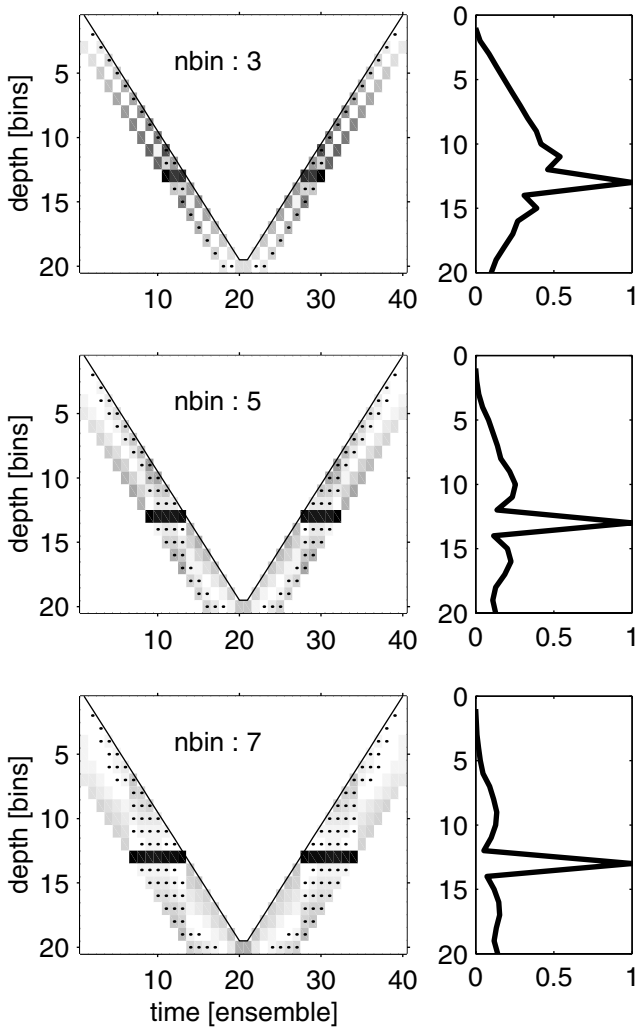
nbin : 3
nbin : 5
nbin : 7
depth [bins]
time [ensemble]
5
10
15
20
30
40
0
0.5
1

Figure 6

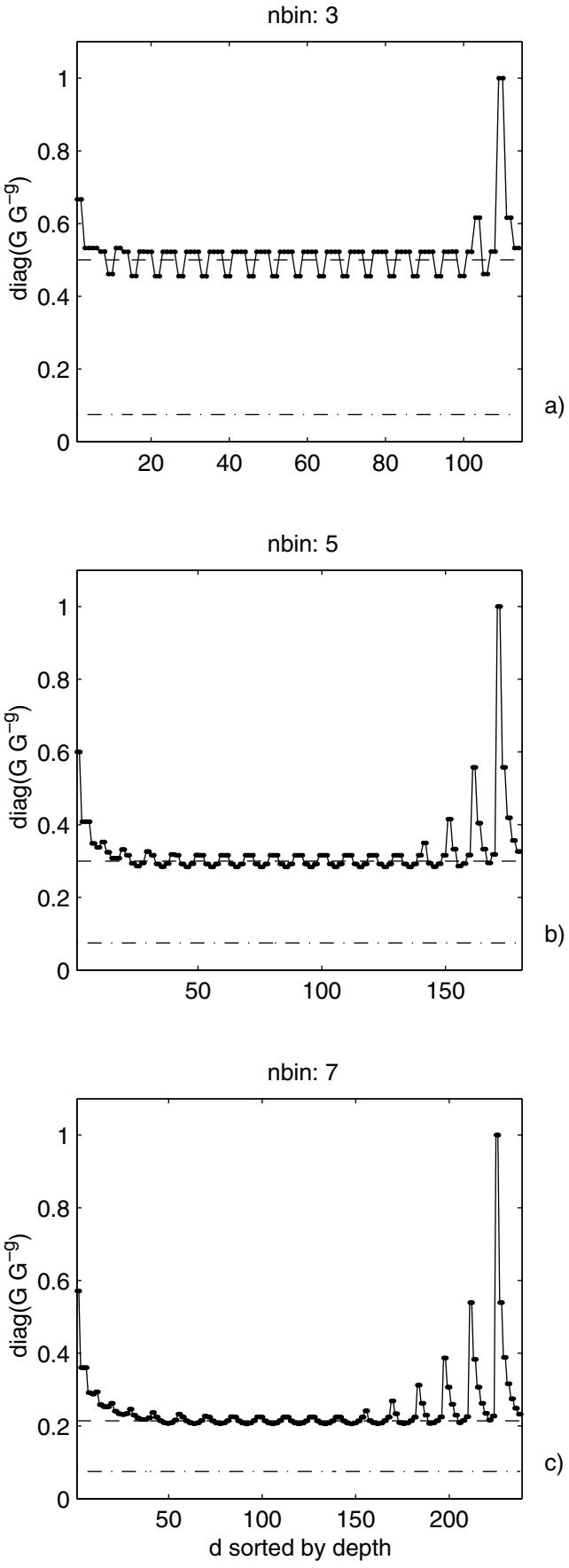
nbin: 3
diag(G G^{-9})
a)
nbin: 5
diag(G G^{-9})
b)
nbin: 7
diag(G G^{-9})
c)
d sorted by depth

Figure 7

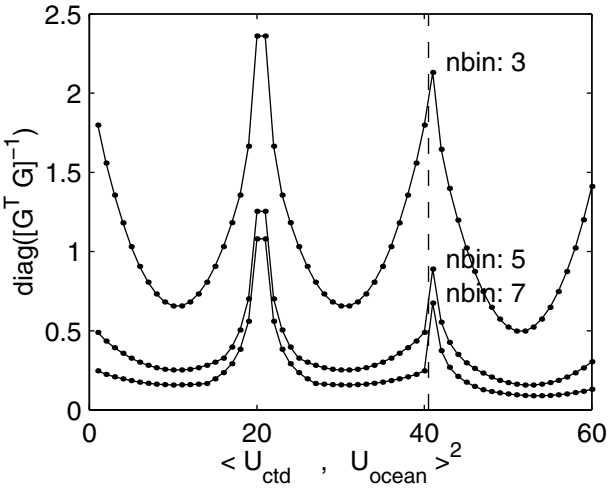
2.5
2
1.5
1
0.5
0
0
20
40
60
diag([G^T G]^-1)
< U_ctd , U_ocean >^2
nbin: 3
nbin: 5
nbin: 7

Figure 8

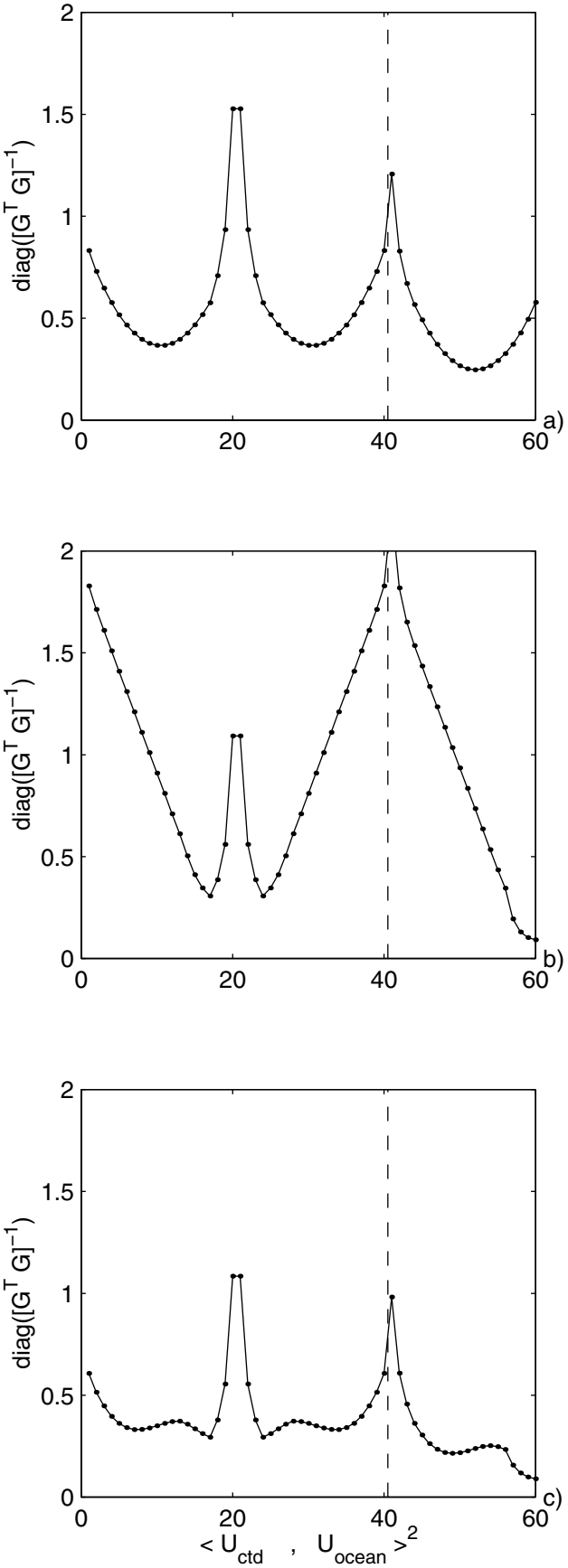

Figure 9

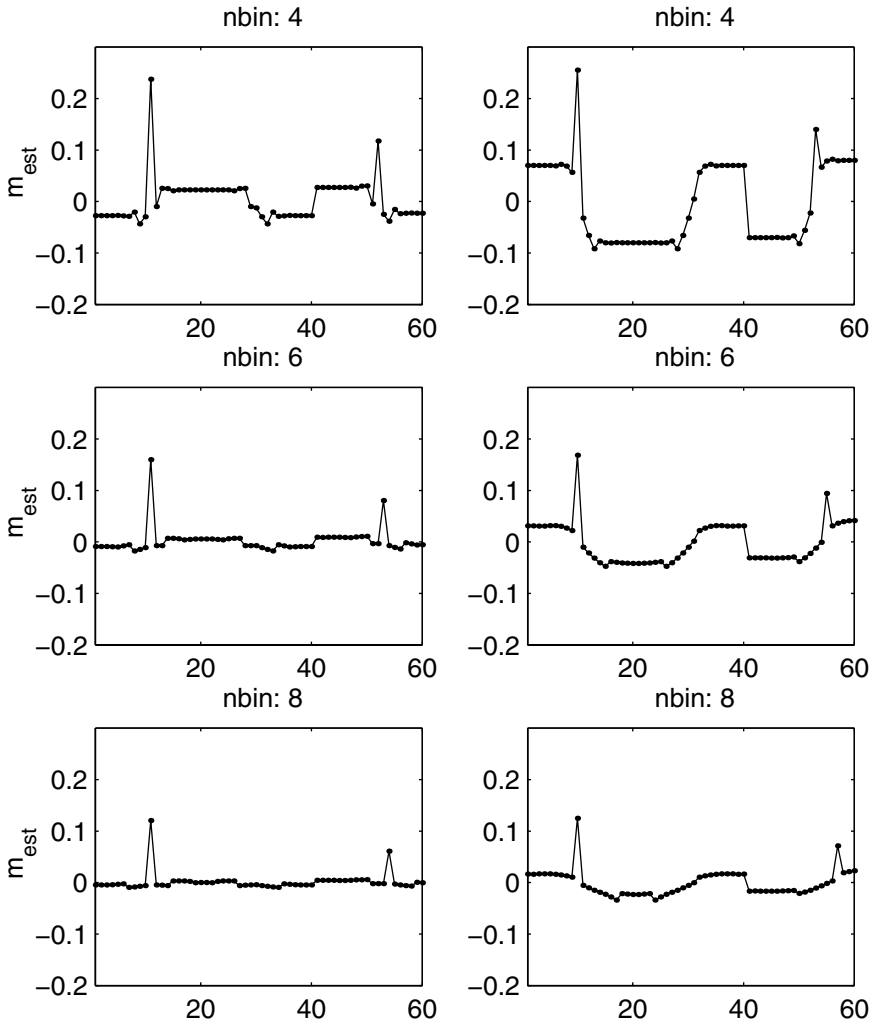

Figure 10

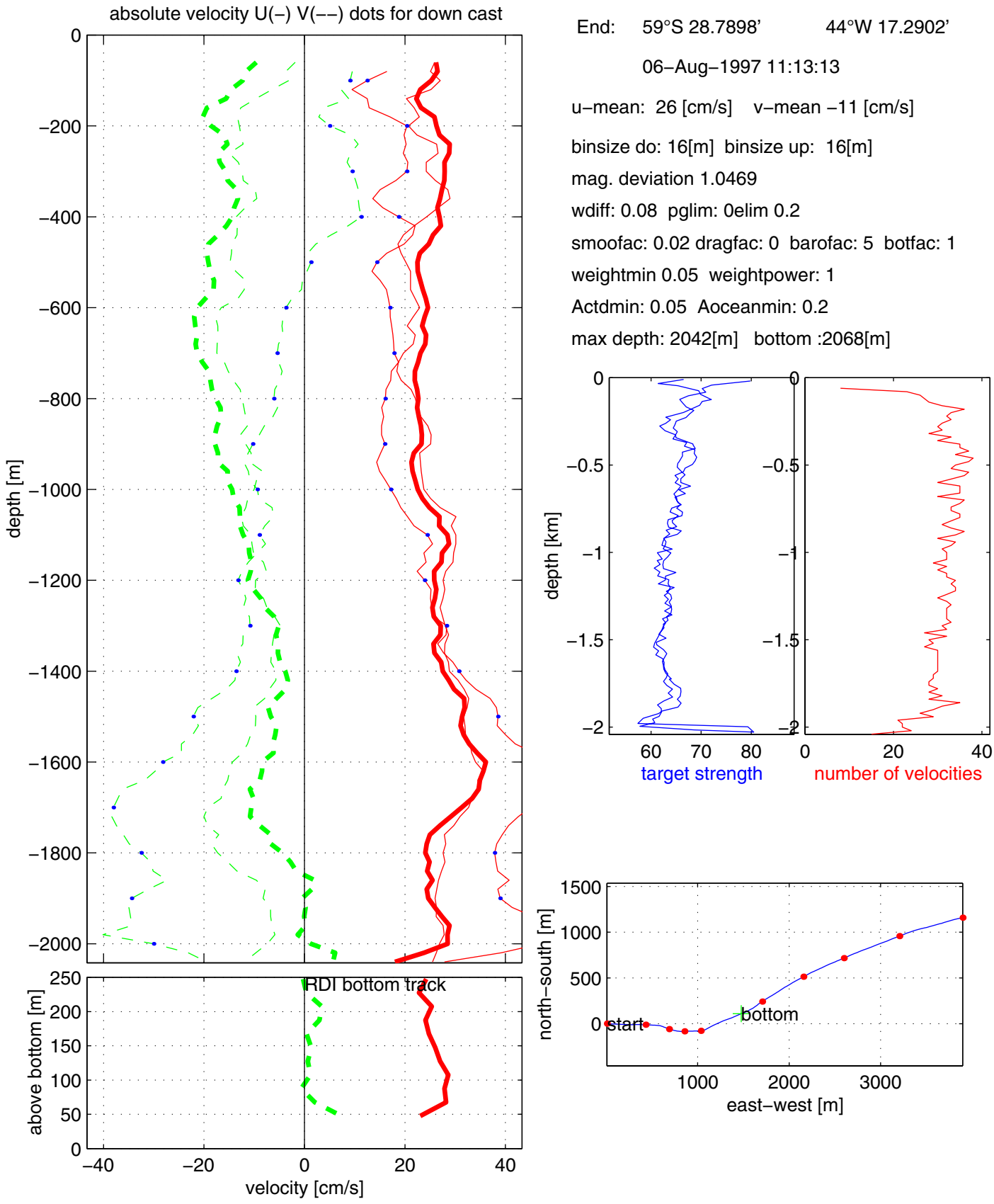
Station : demo–data
Start: 59°S 29.4202' 44°W 21.4800'
06–Aug–1997 09:22:22
End: 59°S 28.7898' 44°W 17.2902'
06–Aug–1997 11:13:13
u–mean: 26 [cm/s] v–mean –11 [cm/s]
binsize do: 16[m] binsize up: 16[m]
mag. deviation 1.0469
wdiff: 0.08 pglim: 0elim 0.2
smoofac: 0.02 dragfac: 0 barofac: 5 botfac: 1
weightmin 0.05 weightpower: 1
Actdmin: 0.05 Aoceanmin: 0.2
max depth: 2042[m] bottom :2068[m]
absolute velocity U(–) V(––) dots for down cast
depth [m]
velocity [cm/s]
RDI bottom track
above bottom [m]
depth [km]
target strength
number of velocities
north–south [m]
east–west [m]
start
bottom

Figure 11